

Contrastive Flow Matching

George Stoica^{1,2†} Vivek Ramanujan^{2‡} Xiang Fan^{2‡}
Ranjay Krishna² Judy Hoffman¹

¹Georgia Tech ²University of Washington

[†]Correspondence to: gstoica3@gatech.edu [‡]Equal Contribution



Figure 1. **Training with Contrastive Flow-Matching (CFM) improves natural image generation.** (left is baseline, right is with CFM) Here we show comparisons between images generated by diffusion models trained on ImageNet-1k (512×512). Each pair of images is generated with the same class and initial noise to ensure similar image structure for comparability. We see that our CFM objective encourages significantly more coherent images and improves the consistency of global structure.

Abstract

Unconditional flow-matching trains diffusion models to transport samples from a source distribution to a target distribution by enforcing that the flows between sample pairs are unique. However, in conditional settings (e.g., class-conditioned models), this uniqueness is no longer guaranteed: flows from different conditions may overlap, leading to more ambiguous generations. We introduce Contrastive Flow Matching (CFM), an extension to the flow-matching objective that explicitly enforces uniqueness across all conditional flows, enhancing condition separation. Our approach adds a contrastive objective that maximizes dissimilarities between predicted flows from arbitrary sample pairs. We validate Contrastive Flow Matching by conducting extensive experiments across varying SiT model sizes on the popular ImageNet-1 (256×256) and (512×512) benchmarks. Notably, we find that training models with CFM (1) improves training speed by a factor of up to $9\times$, (2) requires up to $5\times$ fewer de-noising steps and (3) lowers FID by up to 8.9 compared to training the same models with flow-matching.

1. Introduction

Flow matching for generative modeling trains continuous normalizing flows by regressing ideal probability flow fields

between a base (noise) distribution and the data distribution [23]. This approach enables straight-line generative trajectories and has demonstrated competitive image synthesis quality. However, for conditional generation (e.g., class-conditional image generation), vanilla flow matching models often produce outputs that resemble an “average” of the possible images for a given condition, rather than a distinct mode of that condition. In essence, the model may collapse multiple diverse outputs into a single trajectory, yielding samples that lack the expected specificity and diversity for each condition [27, 41]. By contrast, an unconditional flow model—tasked with covering the entire data distribution without any conditioning—implicitly learns more varied flows for different modes of the data. Existing conditional flow matching formulations *do not enforce the flows to differ across conditions*, which can lead to this averaging effect and suboptimal generation fidelity.

To address these limitations and improve generation quality, recent work has explored enhancements to structure the generator’s representations and also proposed inference-time guidance strategies. For example, one approach is to incorporate a *REpresentation Alignment* (REPA) objective to structure the representations at an intermediate layer with those from a high-quality pretrained vision encoder [41]. By using feature embeddings from a DINO self-supervised vision transformer [4, 29], the generative model’s hidden states

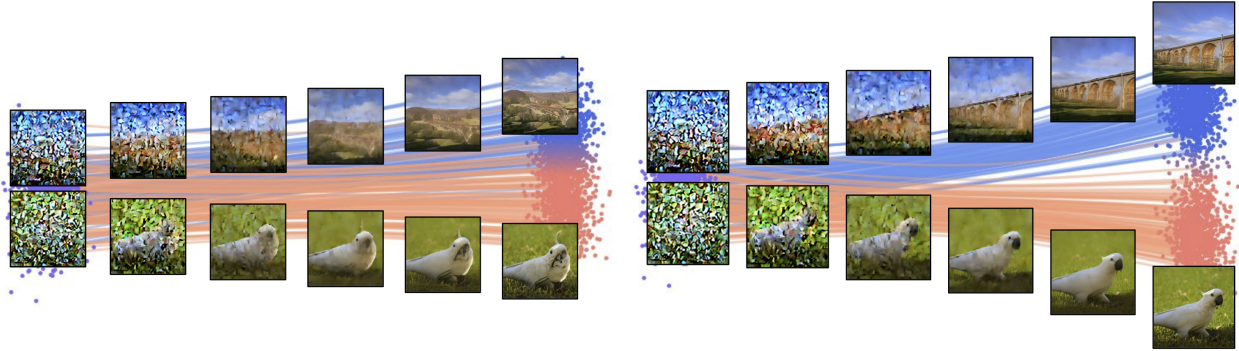


Figure 2. **CFM yields more discriminative and higher quality trajectories.** (left) shows the result of standard flow-matching, where flows are straight but end up overlapping for similar class distributions. (right) shows how the addition of the CFM objective results in more distinct flows, resulting in images which are more representative of their respective classes.

are guided toward semantically meaningful directions. This representational alignment provides an additional learning signal that has been shown to improve both training convergence and final image fidelity, albeit at the cost of requiring an external pretrained encoder and an auxiliary loss term. Another popular technique is *classifier-free guidance* (CFG) for conditional generation [16], which involves jointly training the model in unconditional and conditional modes (often by randomly dropping the condition during training). At inference time, CFG performs two forward passes—one with the conditioning input and one without—and then extrapolates between the two outputs to push the sample closer to the conditional target [16, 27]. While CFG can significantly enhance image detail and adherence to the prompt or class label, it doubles the sampling cost and complicates training by necessitating an implicit unconditional generator alongside the conditional ones [10, 10, 18].

We propose **Contrastive Flow Matching** (CFM), a new approach that augments the flow matching objective with an auxiliary contrastive learning objective. CFM encourages more diverse and distinct conditional generations. It applies a contrastive loss on the flow vectors (or representations) of samples within each training batch, encouraging the model to produce dissimilar flows for different conditioning inputs. Intuitively, this loss penalizes the model if two samples with different conditions yield similar flow dynamics, thereby explicitly discouraging the collapse of multiple conditions onto a single “average” generative trajectory. As a result, given a particular condition, the model learns to generate a unique flow through latent space that is characteristic of that condition alone, leading to more varied and condition-specific outputs. Importantly, this contrastive augmentation is *complementary* to existing methods. It can be applied along with REPA, further ensuring that flows not only align with pretrained features but also remain distinct across conditions. Likewise, it is compatible with classifier-free guidance at sampling time, allowing one to combine its benefits with

CFG for even stronger conditional signal amplification.

Inspired by contrastive training objectives, CFM applies a pairwise loss term between samples in a training batch: for each positive sample from the batch, we randomly sample a negative counterpart. We then encourage the model to not only learn the flow towards the positive sample but also to learn the flow away from the negative sample. This is achieved by adding a contrastive loss to the flow-matching objective, which promotes class separability throughout the flow. Our method is simple to implement and can be easily integrated into existing diffusion models without any additional data and with minimal computational overhead.

We validate the advantages of CFM through extensive experiments on conditional image generation using ImageNet images across multiple SiT [27] model scales and training frameworks [27, 41]. Thanks to contrastive flows, CFM consistently outperforms traditional diffusion flow-matching in quality and diversity metrics, achieving up to an 8.9-point reduction in FID-50K. It is also compatible with recent significant improvements in the diffusion objective, such as Representation Alignment (REPA) [41]. By encouraging class separability, CFM is able to efficiently reach a given image quality with $5\times$ **fewer** sampling steps than a baseline Flow Matching model, translating directly to faster generation. It also enhances training efficiency by up to $9\times$. In summary, our findings advance the field of diffusion-based image generation by achieving state-of-the-art performance.

2. Related works

Our work lies in the domain of image generative models, primarily diffusion and flow matching models. We augment flow matching with a contrastive learning objective to provide an alternative solution to classifier free guidance.

Generative modeling has rapidly advanced through two primary paradigms: diffusion-based methods [17, 36] and flow matching [23]. **Denoising diffusion models** typically rely on stochastic differential equations (SDEs) and score-

based learning to iteratively add and remove noise [17]. Denoising diffusion implicit models (DDIMs) [36] reduce this sampling complexity by removing non-determinism in the reverse process, while progressive distillation [32] further accelerates inference by shortening the denoising chain. Advanced ODE solvers [5] and distillation methods [38] have also enhanced sampling efficiency. Despite their success, diffusion models can be slow at inference due to iterative denoising [17].

Flow matching [5] has been designed to reduce inference steps. It directly parameterizes continuous-time transport dynamics for more efficient sampling. Probability flow ODEs [23, 36] learn an explicit transport map between data and latent distributions. Unlike diffusion models, it bypasses separate score estimation and stochastic noise, which reduces function evaluations and tends to improve training convergence [5]. A common type of flow matching algorithm popularized recently is the rectified flow [24], which refines probability flow ODEs through direct optimal transport learning, improving numerical stability and sampling speed. This approach mitigates the high computational burden of diffusion sampling while maintaining high-fidelity image generation with fewer integration steps.

Since both diffusion and flow matching models are trained to match the target distribution of real images, they often produce ‘averaged’ samples that lack the sharp details and strong conditional fidelity [15]. Regardless of how much these models speed up, they often need to be invoked multiple times with unique seed noise to find a high-fidelity sample. In response, **guidance techniques** have been introduced to substantially promote high-fidelity synthesis. Classifier guidance [11], classifier-free guidance [15], energy guidance [7, 25, 37, 42], and more advanced methods [8, 18, 19, 21, 35] improve fidelity and controllability, without requiring multiple invocations. Although they achieve remarkable performance, they typically still require additional computational overhead. CFG requires calling sampling from a second ‘unconditional’ generation and guiding the ‘conditional’ generation away from the unconditional variant [26, 39, 40, 43]. We adapt the flow matching objective with a contrastive loss between the transport vectors within a batch. By doing so, we achieve the same benefits of CFG, without the additional overhead of needing to train an unconditional generator or using one during inference.

Contrastive learning was originally proposed for face recognition [34], where it was designed to encourage a margin between positive and negative face pairs. In generative adversarial networks (GANs), it has been applied to improve sample quality by structuring latent representations [3]. However, to the best of our knowledge, it has not been explored in the context of visual diffusion or flow matching models. We incorporate this contrastive objective to demonstrate its utility in speeding up training and inference of flow-based

generative models.

3. Background and motivation

We focus on flow-matching models [23] due to its rising popularity as an effective training paradigm for generative models [1, 2, 22]. In this section, we provide a brief overview of flow-matching through the perspective of stochastic interpolants [2, 27], as it pertains to our work.

Preliminaries. Let $p(x)$ be an arbitrary distribution defined on the reals, and let $\mathcal{N}(0, 1)$ be a Gaussian noise distribution. The objective of flow-matching is to learn a transport between the two distributions. That is, given an arbitrary $\epsilon \sim \mathcal{N}(0, 1)$, a flow-matching model gradually transforms ϵ over time into an \hat{x} that is part of $p(x)$. Stochastic interpolants [2, 27] define this transformation as a time-dependent stochastic process, where transformation steps are summarized as follows,

$$\hat{x}_t = \alpha_t \hat{x} + \sigma_t \epsilon \quad (1)$$

where α_t and σ_t are decreasing and increasing time-dependent functions respectively defined on $t \in [0, T]$, such that $\alpha_T = \sigma_0 = 1$ and $\alpha_0 = \sigma_T = 0$. While theoretically, α_t, σ_t need not be linear, linear complexity is often sufficient to obtain strong diffusion models [23, 27, 41].

Flow-matching. Given such a process, flow-matching models learn to transport between noise to $p(x)$ by estimating a velocity field over an probability flow ordinary differential equation (PF ODE), $dx_t = v(x_t, t)dt$, whose distribution at time t is the marginal $p_t(x)$. This velocity is given by the expectations of \hat{x} and ϵ conditioned on x_t ,

$$v(x_t, t) = \dot{\alpha}_t \mathbb{E}[\hat{x}|x_t = x] + \dot{\sigma}_t \mathbb{E}[\epsilon|x_t = x], \quad (2)$$

where $\dot{\alpha}_t, \dot{\sigma}_t$ are the time-based derivatives of α_t and σ_t respectively. Since, \hat{x} and ϵ are arbitrary samples from their respective distributions, $v(x_t, t)$ is expected “direction” of all transport paths between noise and $p(x)$ that pass through x_t at t . While the optimal $v(x_t, t)$ is intractable, it can be approximated with a flow-model $v_\theta(x_t, t)$, by minimizing the training objective:

$$\mathcal{L}^{(FM)}(\theta) = \mathbb{E} [\|v_\theta(x_t, t) - (\dot{\alpha}_t \hat{x} + \dot{\sigma}_t \epsilon)\|^2] \quad (3)$$

Key to understanding the properties of flow-matching is the concept of flow uniqueness [23]. That is, flows following the well-defined ODE cannot intersect at *any* time $t \in [0, T]$. As such, flow models can iteratively refine unique-discriminative features relevant to any $x \sim p(x)$ in each x_t , leading to more efficient and accurate diffusion paths compared to other training paradigms [23].

Conditional flow-matching. Commonly, $p(x)$ may be a marginal distribution over several class-conditional distributions (e.g., the classes of ImageNet [31]). Training models

in such cases is nearly identical to standard flow-matching, except that flows are further conditioned on the target distribution class:

$$\mathcal{L}_{cond}^{(FM)}(\theta) = \mathbb{E} [\|v_\theta(x_t, t, y) - (\dot{\alpha}_t \hat{x} + \dot{\sigma}_t \epsilon)\|^2], \quad (4)$$

where $\hat{x} \sim p(x|y)$. Resultant models have the desirable trait of being more controllable: their generated outputs can be tailored to their respective input conditions. However, this comes at the notable cost of flow-uniqueness. Specifically these models only generate unique flows compared to others *within* the same class-condition, not necessarily *across* classes. This inhibits x_t 's from storing important class-specific features and leads to poorer quality generations. Second, the conditional flow-matching objective trains models without knowledge of the distributional spread from other class-conditions, leading to flows that may generate ambiguous outputs when conditional distributions overlap. This increases the likelihood of ambiguous generations that form a mixture between different conditions, restricting model capabilities. We study these effects in Section 5.

4. Contrastive Flow Matching

We introduce Contrastive Flow-Matching (CFM), a novel approach designed to address the challenges of learning efficient class-distinct flow representations in conditional generative models. Standard conditional flow-matching (FM) models tend to produce flow trajectories that align across different samples, leading to reduced class separability. CFM extends the FM objective by incorporating a contrastive regularization term, which explicitly discourages alignment between the learned flow trajectories of distinct samples.

Ingredients. Let $\tilde{x} \sim p(x|\tilde{y})$ denote a sample drawn from the data distribution conditioned on an arbitrary class \tilde{y} , and let $\tilde{\epsilon} \sim \mathcal{N}(0, I)$ represent an independent noise sample. To ensure that the contrastive objective captures distinct flow trajectories, we impose the conditions $\tilde{x} \neq \hat{x}$ and $\tilde{\epsilon} \neq \epsilon$, where \tilde{y} may or may not be equal to y . Importantly, we do not assume the existence of a time step $t \in [0, T]$ such that $x_t = \alpha_t \tilde{x} + \sigma_t \tilde{\epsilon}$. Consequently, \tilde{x} and $\tilde{\epsilon}$ represent truly independent flow trajectories in comparison to \hat{x} and ϵ .

The contrastive regularization. Given $v_\theta(x_t, t, y)$ and an arbitrary $\tilde{x}, \tilde{\epsilon}$ sample pair, the contrastive objective aims to *maximize* the dissimilarity between the estimated flow of $v_\theta(x_t, t, y)$ from ϵ to \hat{x} , and the independent flow produced by $\tilde{x}, \tilde{\epsilon}$. We achieve this by maximizing the quantity,

$$E [\|v_\theta(x_t, t, y) - (\dot{\alpha}_t \tilde{x} + \dot{\sigma}_t \tilde{\epsilon})\|^2]. \quad (5)$$

Since \tilde{x} is drawn from the marginal $p(x)$ rather than $p(x|y)$, Equation 5 trains flow-matching models to produce flows that are *unconditionally* unique.

Putting it all together. We now define contrastive flow-matching as follows,

$$\mathcal{L}^{(CFM)}(\theta) = E \left[\begin{aligned} & \|v_\theta(x_t, t, y) - (\dot{\alpha}_t \hat{x} + \dot{\sigma}_t \epsilon)\|^2 \\ & - \lambda \|v_\theta(x_t, t, y) - (\dot{\alpha}_t \tilde{x} + \dot{\sigma}_t \tilde{\epsilon})\|^2 \end{aligned} \right] \quad (6)$$

where $\lambda \in [0, 1)$ is a fixed hyperparameter that controls the strength of the contrastive regularization. Thus, CFM simultaneously encourages flow-matching models to estimate effective transports from noise to corresponding class-conditional distributions (the flow-matching objective), while enforcing each to be discriminative *across* classes (contrastive regularization). Note that CFM can be thought of as a generalization of flow-matching, as CFM reduces to FM when $\lambda = 0$. We study the effects of varying λ in Section 5.4.

Implementation. Contrastive flow-matching (CFM) is easily integrated into any flow-matching training loop, with minimal overhead. Algorithm 1 illustrates the implementation of an arbitrary batch step, where **navy text** marks additions to the standard flow-matching objective. Thus, CFM solely depends on the information already available to the flow-matching objective at each batch step, without computing any additional forward steps. Furthermore, CFM seamlessly folds into flow-matching training regimes, making it a “plug-and-play” objective for existing setups.

Algorithm 1 Contrastive Flow-Matching Batch Step

- 1: **Input:** A model v_θ , batch of N flow examples $F = \{(x_1, y_1, \epsilon_1), \dots, (x_N, y_N, \epsilon_N)\}$ where $(x_i, y_i) \sim p(x, y)$ and $\epsilon_i \sim \mathcal{N}(0, I)$, β learning rate, $\lambda = 0.05$.
 - 2: **Output:** Updated model parameters θ
 - 3: $L(\theta) = 0$
 - 4: **for** i in range(N) **do**
 - 5: $t \sim U(0, 1), x_t = \alpha_t x_i + \sigma_t \epsilon_i$
 - 6: **sample** $(\tilde{x}, \tilde{y}, \tilde{\epsilon}) \sim F$, s.t. $(\tilde{x}, \tilde{y}, \tilde{\epsilon}) \neq (x_i, y_i, \epsilon_i)$
 - 7: $\hat{v} = v_\theta(x_t, t, y_i), v = \dot{\alpha}_t x_i + \dot{\sigma}_t \epsilon_i, \tilde{v} = \dot{\alpha}_t \tilde{x} + \dot{\sigma}_t \tilde{\epsilon}$
 - 8: $L(\theta) += \| \hat{v} - v \|^2 - \lambda \| \hat{v} - \tilde{v} \|^2$
 - 9: **end for**
 - 10: $\theta \leftarrow \theta - \frac{\beta}{N} \nabla_\theta L(\theta)$
-

Discussion. Figure 3 illustrates the effects of contrastive flow-matching compared to flow-matching. The figure shows the resultant flows after training a small diffusion model in a simple toy-setting. Specifically, we create a two-dimensional **violet** gaussian noise distribution and two independent two-dimensional class distributions (in **blue** and **orange** respectively) such that the latter distributions have $\approx 50\%$ overlap. Samples from each distribution are represented as “dots”, with those in the target distributions colored according to the gaussian *kernel-density estimate* between samples from each class in their respective region.

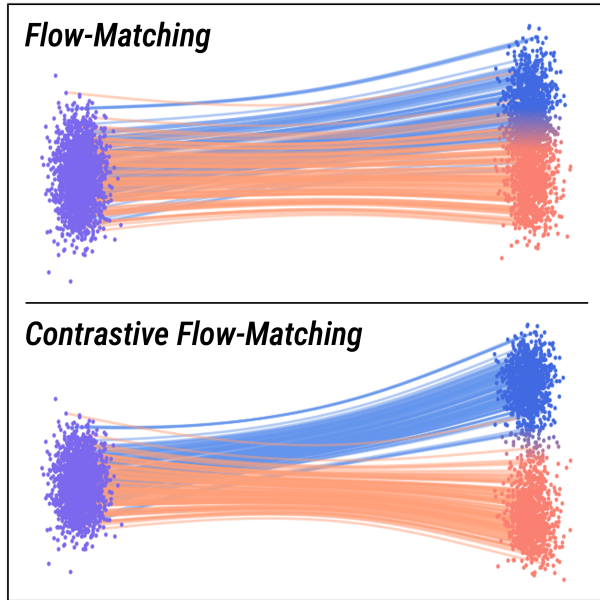


Figure 3. **Contrastive Flow-Matching intrinsically separates flows between classes.** We train a small three layer MLP flow-matching model to transport between a two dimensional multivariate noise distribution (violet) and two independent blue and orange class distributions respectively. The class distributions are designed to have $\sim 50\%$ overlap, and we plot the learned class-conditioned flows between noise samples and each respective class distribution using class colors. Top: Flow-matching models learn overlapping transports between distributions, generating outputs that lie in ambiguous regions between the two classes. Bottom: Contrastive flow-matching models have significantly more discriminative flows, generating class-coherent samples while reducing ambiguity.

We observe that training the model with flow-matching (top) create flows with large degrees of overlap between classes, generating samples with lower class-distinction. In contrast, training the same model with contrastive flow-matching (bottom) yields trajectories that are significantly more diverse across classes, while also generating samples which capture distinct features of each respective class.

5. Experiments

We validate contrastive flow-matching (CFM) through extensive experiments across various model, training and benchmark configurations. Overall, models trained with CFM consistently outperform flow-matching (FM) models across *all* settings.

Datasets. We use ImageNet-1k [9] processed at both (256×256) and (512×512) resolutions, and follow the data preprocessing procedure of ADM [11]. We then follow [41] and encode each image using the Stable Diffusion VAE [30] into a tensor $z \in \mathbb{R}^{32 \times 32 \times 4}$. We train all models by strictly following the setup in [41], and use a batch size

of 256 unless otherwise specified. We do not alter the training conditions to be favorable to CFM, and we always set $\lambda = 0.05$ when applicable.

Measurements. We report five quantitative metrics throughout our experiments. Specifically, we report Frchet inception distance (FID) [14], inception score (IS) [33], sFID [28], precision (Prec.) and recall (Rec.) [20] using 50,000 samples. We use the SDE Euler-Maruyama sampler with $w_t = \sigma_t$ for all experiments, and set the number of function evaluations (NFE) to 50 unless otherwise specified.

5.1. Contrastive Flow-Matching Improves SiT

Implementation details. We train on the state-of-the-art SiT [27] model architecture, using both SiT-B/2 and SiT-XL/2.

Model	Metrics				
	FID ↓	IS ↑	sFID ↓	Prec. ↑	Rec. ↑
SiT-B/2	42.28	38.04	11.35	0.5	0.62
+ Using CFM	33.39	43.44	5.67	0.53	0.63
SiT-XL/2	20.01	74.15	8.45	0.63	0.63
+ Using CFM	16.32	78.07	5.08	0.66	0.63

(a) **ImageNet-1k (256x256) Results.** CFM significantly outperforms flow-matching models across nearly all metrics, and matches Recall on SiT-XL/2.

Model	Metrics				
	FID ↓	IS ↑	sFID ↓	Prec. ↑	Rec. ↑
SiT-B/2	50.26	33.58	14.88	0.57	0.61
+ Using CFM	41.59	38.20	6.13	0.62	0.63
SiT-XL/2	22.98	70.14	10.71	0.73	0.60
+ Using CFM	19.67	72.58	4.98	0.76	0.60

(b) **ImageNet-1k (512x512) Results.** Models trained with CFM either substantially outperform or match their flow-matching counterparts in all metrics.

Table 1. SiT [27] results on ImageNet-1k (256×256) ; a) and (512×512) ; b). We train all models for 400K iterations following [41]. All metrics are measured with the SDE Euler-Maruyama sampler with NFE=50 and without classifier guidance. We use $\lambda = 0.05$ for all models trained with CFM and do not change any other hyperparameters. \uparrow indicates that higher values are better, with \downarrow denoting the opposite.

Table 1 summarizes our results. Overall, CFM dramatically improves over flow-matching in nearly all metrics (only matching the flow-matching SiT-XL/2 model in recall). Notably, employing CFM with SiT-B/2 lowers FID by over 8 compared to flow-matching at both ImageNet resolutions, highlighting the strength of CFM in smaller model scales. Similarly, CFM is robust to larger model scales and outperforms FM by over 3.2 FID when using SiT-XL/2.

5.2. REPA is complementary

REPresentation Alignment (REPA) [41] is a recently introduced training framework that rapidly improves diffusion model performance by strengthening its intermediate representations. Specifically, REPA distills the encodings of foundation vision encoders (e.g., DiNOv2 [4]) into the hidden states of diffusion models through the use of an auxiliary objective. Notably, REPA can improve the training speed of vanilla SiT models by over $17.5\times$, while further improving their performances [41]. CFM is easily integrated into REPA and only requires replacing the flow-matching objective.

Implementation details. We apply REPA on the same SiT models as in Section 5.1, and use the distillation process defined by [41] exactly. Specifically, we use distill DiNOv2 [4] ViT-B [12] features into the 4th layer of the SiT-B/2, and the 8th layer of the SiT-XL/2, and mirror their hyperparameter setup.

Model	Metrics				
	FID ↓	IS ↑	sFID ↓	Prec. ↑	Rec. ↑
REPA SiT-B/2	27.33	61.60	11.70	0.57	0.64
+ Using CFM	20.52	69.71	5.47	0.61	0.63
REPA SiT-XL/2	11.14	115.83	8.25	0.67	0.65
+ Using CFM	7.29	129.89	4.93	0.71	0.64

(a) **ImageNet-1k (256x256) Results with REPA.** Adding CFM to REPA further improves SiT models across nearly all metrics, and by as much as 6.81 FID.

Model	Metrics				
	FID ↓	IS ↑	sFID ↓	Prec. ↑	Rec. ↑
REPA SiT-B/2	31.90	56.96	13.78	0.67	0.62
+ Using CFM	24.48	64.74	5.89	0.71	0.61
REPA SiT-XL/2	11.32	119.72	10.21	0.76	0.63
+ Using CFM	7.64	131.50	4.72	0.79	0.62

(b) **ImageNet-1k (512x512) Results with REPA.** CFM is robust with REPA at large image resolutions, further improving performance across established metrics.

Table 2. REPA SiT [27] results on ImageNet-1k (256×256 ; a) and (512×512 ; b). All models are trained for 400K iterations strictly following the procedure in [41], and set $\lambda = 0.05$. We use the SDE Euler-Maruyama sampler with NFE=50 without classifier guidance for all our metrics.

We report results in Table 2. Similar to Section 5.1, CFM substantially improves REPA models by as much as 6.81 FID, and consistently improves flow-matching with model scale. This highlights the versatility of the contrastive flow-matching objective as a broadly applicable criterion for diffusion model.

Metric	CFG Scale			
	No CFG	1.75	1.80	1.85
IS ↑	131.50	255.68	262.23	268.39
FID ↓	7.64	2.18	2.17	2.19

Table 3. **ImageNet 256x256 Results with CFG.** Integrating Contrastive Flows (CF) with Classifier-Free Guidance (CFG) enhances FID, IS, and sFID scores during inference, demonstrating the potential for further performance improvements in our model with the use of CFG.

Metric	CFM λ Values					
	0.0	0.001	0.01	0.05	0.1	0.15
IS ↑	115.83	115.70	119.41	129.89	116.27	82.20
FID ↓	11.14	10.93	9.93	7.29	9.86	19.21

Table 4. $\lambda = 0.05$ is **ideal**. We show an ablation of the CFM weight parameter λ . A too large λ produces degenerate distributions that do not model class structure well. Too low λ is essentially identical to flow-matching, with very little effect on training. $\lambda = 0.05$ is best and we use this for all our experiments.

5.3. CFG Stacks with Contrastive Flow-Matching

Contrastive flow-matching offers advantages of Classifier-Free Guidance (CFG), without incurring additional computational costs during inference. In this section, we demonstrate that when computational resources permit, combining CFM with CFG can yield further performance enhancements. We use our CFM REPA SiT-XL/2 model trained on the training set of ImageNet-1k (256×256), and evaluate its performance as in Section 5.2. Our evaluation sets NFE=50, with $\sigma_{\text{high}} = 0.65$, and the results are presented in Table 3. We find that integrating CFM with CFG enhances FID, IS, and sFID scores during inference. This suggests that CFM retains the capability to leverage CFG for improved performance when computational costs are not a constraint, thereby further boosting the model’s efficacy.

5.4. Analyzing Contrastive Flow-Matching

Understanding the CFM weight (λ). λ directly controls how unique flows are across classes. Increasing λ encourages every diffusion step to be fully discriminative, enabling models to encode distinct representations that integral to generating strong visual outputs at each trajectory step. However, setting it too high can lead to overly-separated flow trajectories, making it difficult to capture the class structure (Table 5.4). However, λ values that are too low mirror the flow-matching objective. Notably, we find that $\lambda = 0.05$ is stable across all model and dataset settings, consistently achieving strong performance.

Earlier class differentiation during denoising. In Figure 4, we study flow trajectories of standard flow-matching (FM)

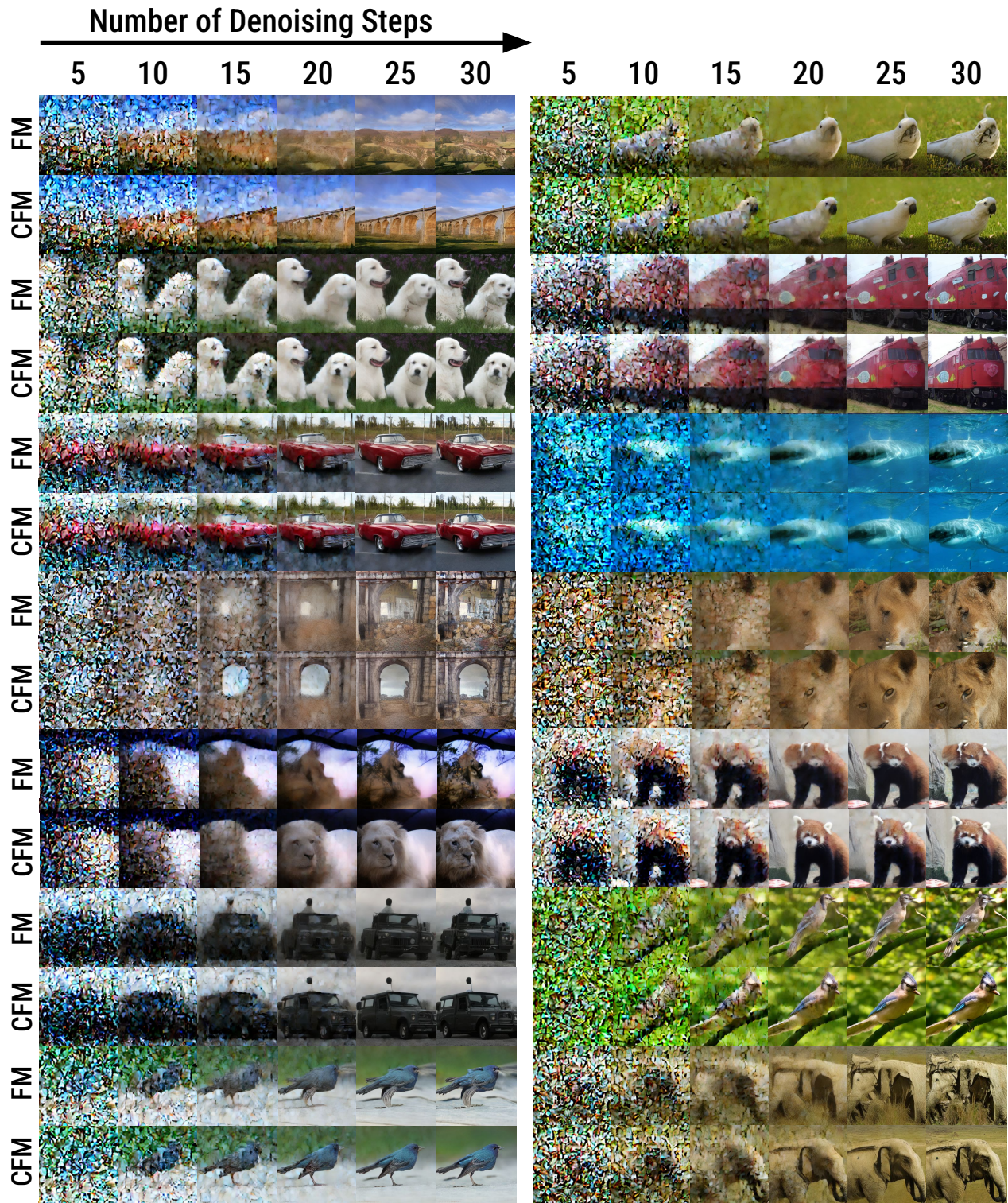


Figure 4. **Contrastive flow-matching (CFM) denoises significantly more efficiently than flow-matching.** We visualize the expected final image estimated by a flow-model when denoised every 5 steps for trajectories of length 30 steps using the SDE Euler-Maruyama sampler and do not use classifier guidance. We compare the trajectories of a REPA SiT-XL/2 [41] trained on ImageNet-256 [9] for 400K steps with flow-matching (FM), and the same model trained with the contrastive flow-matching (CFM) objective. We show these trajectories in sets of pairs generated from the same noise sample during inference, with the flow-matching model above our CFM version.

and flow-matching with CFM. To do this, we take partially denoised latents at various intermediate time steps along a trajectory with total length 30. While initially both follow similar trajectories, they quickly diverge within the first several steps of the denoising process. For instance, the model trained with CFM produces more structurally coherent images earlier (around 15 to 20 steps in) than with FM. The iconic features of each class, such as slanted bridge surfaces (Figure 4 (top-left)), animal eyes (Figure 4 (upper-left and top-right)), and train windows (Figure 4 (upper-right)), are more clearly visible early on during the diffusion process of the CFM model. This enables CFM to ultimately generate higher quality images at the final timestep.

Effects of batch size on CFM. In Table 5.4, we study the effects of batch size on our loss. It is well known that batch size has an important effect on contrastive style losses [4, 6, 13] that draw negatives within the batch. This can be understood as a sample diversity issue. If the batch size is larger than negative samples within the batch are more representative of the true distribution. In this table, we see a similar trend: larger batch sizes are important for maximizing the performance of CFM across several model scales. We also maintain our improvements over the REPA baseline through all batch sizes and model scales.

Improved training and inference speed. In Figure 5 (left), we see the significant improvements in training speed from the CFM objective. We reach the same performance (measured by FID-50k) as baseline after half the number of training iterations. In Figure 5 (right), we also demonstrate significant improvements at inference time. With our objective, we reach superior performance with only 50 denoising steps compared to the baseline with 250 denoising steps. This is a linear $5\times$ improvement in training efficiency. Taken together, these results emphasize the important gains in computational efficiency achieved by our method.

6. Conclusion

We introduced Conditional Flow Matching (CFM), a simple addition to the diffusion objective that enforces distinct, diverse flows during image generation. Quantitatively, CFM results in improved image quality with far fewer denoising steps ($5\times$ faster) and significantly improved training speed ($2\times$ faster). Qualitatively, CFM improves the structural coherence and global semantics for image generation. All of this is achieved with negligible extra compute per training iteration. Finally, we show that our improvements stack with the recently proposed Representation Alignment (REPA) loss, allowing for strong gains in image generation performance. Looking forward, CFM shows the possibility that deviating from perfect distribution modeling in the diffusion objective might result in better image generation.

Model	Batch Size	Metrics		
		FID ↓	IS ↑	sFID ↓
REPA SiT-B/2	256	42.28	38.04	11.35
+ Using CFM	256	33.39	43.44	5.67
REPA SiT-B/2	512	24.45	69.15	11.42
+ Using CFM	512	17.06	81.41	5.29
REPA SiT-B/2	1024	22.00	76.15	11.76
+ Using CFM	1024	15.23	88.53	5.20
REPA SiT-XL/2	256	11.14	115.83	8.25
+ Using CFM	256	7.29	129.89	4.93
REPA SiT-XL/2	512	10.15	129.43	9.00
+ Using CFM	512	6.36	146.17	5.42

Table 5. **CFM Scales with Batch Size.** We train all models for 400K iterations and strictly follow the protocol of [41]. All metrics are measured with the SDE Euler-Maruyama sampler with NFE=50 and without classifier guidance. We use $\lambda = 0.05$ for all models trained with CFM and do not change any other hyperparameters. \uparrow indicates that higher values are better, with \downarrow denoting the opposite. Improvement using CFM evenly scales with batch-size, and even outperforms flow-matching models with *half* the batch-size.

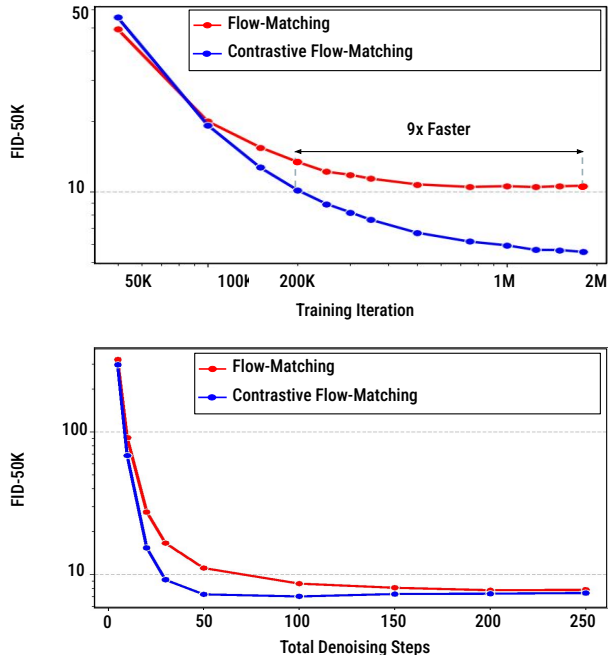


Figure 5. **CFM requires significantly fewer training iterations and inference-time denoising steps.** We plot FID-50k on ImageNet 256x256 with different numbers of training iterations and denoising steps. We see that CFM outperforms the baseline with **9x fewer** training iterations and **5x reduction** in the number of inference-time denoising steps, indicating that CFM is more efficient in both training and inference.

References

- [1] Michael S Albergo and Eric Vanden-Eijnden. Building normalizing flows with stochastic interpolants. *arXiv preprint arXiv:2209.15571*, 2022. 3
- [2] Michael S Albergo, Nicholas M Boffi, and Eric Vanden-Eijnden. Stochastic interpolants: A unifying framework for flows and diffusions. *arXiv preprint arXiv:2303.08797*, 2023. 3
- [3] Gongze Cao, Yezhou Yang, Jie Lei, Cheng Jin, Yang Liu, and Mingli Song. Tripletgan: Training generative model with triplet loss, 2017. 3
- [4] Mathilde Caron, Hugo Touvron, Ishan Misra, Hervé Jégou, Julien Mairal, Piotr Bojanowski, and Armand Joulin. Emerging properties in self-supervised vision transformers. In *ICCV*, 2021. 1, 6, 8
- [5] Ricky T. Q. Chen, Yulia Rubanova, Jesse Bettencourt, and David Duvenaud. Neural ordinary differential equations. In *Advances in Neural Information Processing Systems*, 2018. 3
- [6] Ting Chen, Simon Kornblith, Mohammad Norouzi, and Geoffrey Hinton. A simple framework for contrastive learning of visual representations. *ICLR*, 2020. 8
- [7] Hyungjin Chung, Jeongsol Kim, Michael T Mccann, Marc L Klasky, and Jong Chul Ye. Diffusion posterior sampling for general noisy inverse problems. *arXiv preprint arXiv:2209.14687*, 2022. 3
- [8] Hyungjin Chung, Jeongsol Kim, Geon Yeong Park, Hyelin Nam, and Jong Chul Ye. Cfg++: Manifold-constrained classifier free guidance for diffusion models. *arXiv preprint arXiv:2406.08070*, 2024. 3
- [9] Jia Deng, Wei Dong, Richard Socher, Li-Jia Li, Kai Li, and Li Fei-Fei. Imagenet: A large-scale hierarchical image database. In *2009 IEEE conference on computer vision and pattern recognition*, pages 248–255. Ieee, 2009. 5, 7
- [10] Alakh Desai and Nuno Vasconcelos. Improving image synthesis with diffusion-negative sampling, 2024. 2
- [11] Prafulla Dhariwal and Alexander Nichol. Diffusion models beat gans on image synthesis. *Advances in neural information processing systems*, 34:8780–8794, 2021. 3, 5
- [12] Alexey Dosovitskiy, Lucas Beyer, Alexander Kolesnikov, Dirk Weissenborn, Xiaohua Zhai, Thomas Unterthiner, Mostafa Dehghani, Matthias Minderer, Georg Heigold, Sylvain Gelly, Jakob Szekoreit, and Neil Houlsby. An image is worth 16x16 words: Transformers for image recognition at scale. In *ICLR*, 2021. 6
- [13] Kaiming He, Haoqi Fan, Yuxin Wu, Saining Xie, and Ross Girshick. Momentum contrast for unsupervised visual representation learning. *CVPR*, 2020. 8
- [14] Martin Heusel, Hubert Ramsauer, Thomas Unterthiner, Bernhard Nessler, and Sepp Hochreiter. Gans trained by a two time-scale update rule converge to a local nash equilibrium. *Advances in neural information processing systems*, 30, 2017. 5
- [15] Jonathan Ho and Tim Salimans. Classifier-free diffusion guidance. *arXiv preprint arXiv:2207.12598*, 2022. 3
- [16] Jonathan Ho and Tim Salimans. Classifier-free diffusion guidance, 2022. 2
- [17] Jonathan Ho, Ajay Jain, and Pieter Abbeel. Denoising diffusion probabilistic models. In *Advances in Neural Information Processing Systems*, 2020. 2, 3
- [18] Tero Karras, Miika Aittala, Tuomas Kynkäänniemi, Jaakko Lehtinen, Timo Aila, and Samuli Laine. Guiding a diffusion model with a bad version of itself. *arXiv preprint arXiv:2406.02507*, 2024. 2, 3
- [19] Felix Koulischer, Johannes Deleu, Gabriel Raya, Thomas De-meester, and Luca Ambrogioni. Dynamic negative guidance of diffusion models: Towards immediate content removal. In *Neurips Safe Generative AI Workshop 2024*. 3
- [20] Tuomas Kynkäänniemi, Tero Karras, Samuli Laine, Jaakko Lehtinen, and Timo Aila. Improved precision and recall metric for assessing generative models. *NeurIPS*, 2019. 5
- [21] Tuomas Kynkäänniemi, Miika Aittala, Tero Karras, Samuli Laine, Timo Aila, and Jaakko Lehtinen. Applying guidance in a limited interval improves sample and distribution quality in diffusion models. *arXiv preprint arXiv:2404.07724*, 2024. 3
- [22] Yaron Lipman, Ricky T. Q. Chen, Heli Ben-Hamu, Maximilian Nickel, and Matthew Le. Flow matching for generative modeling. In *ICLR*, 2023. 3
- [23] Yaron Lipman, Ricky T. Q. Chen, Heli Ben-Hamu, Maximilian Nickel, and Matthew Le. Flow matching for generative modeling. In *ICLR*, 2023. 1, 2, 3
- [24] Xingchao Liu, Chengyue Gong, and Qiang Liu. Flow straight and fast: Learning to generate and transfer data with rectified flow, 2022. 3
- [25] Cheng Lu, Huayu Chen, Jianfei Chen, Hang Su, Chongxuan Li, and Jun Zhu. Contrastive energy prediction for exact energy-guided diffusion sampling in offline reinforcement learning. In *International Conference on Machine Learning*, pages 22825–22855. PMLR, 2023. 3
- [26] Simian Luo, Yiqin Tan, Longbo Huang, Jian Li, and Hang Zhao. Latent consistency models: Synthesizing high-resolution images with few-step inference. *arXiv preprint arXiv:2310.04378*, 2023. 3
- [27] Nanye Ma, Mark Goldstein, Michael S. Albergo, Nicholas M. Boffi, Eric Vanden-Eijnden, and Saining Xie. Sit: Exploring flow and diffusion-based generative models with scalable interpolant transformers. 2024. 1, 2, 3, 5, 6
- [28] Charlie Nash, Jacob Menick, Sander Dieleman, and Peter W Battaglia. Generating images with sparse representations. *arXiv preprint arXiv:2103.03841*, 2021. 5
- [29] Maxime Oquab, Timothée Darcet, Théo Moutakanni, Huy V. Vo, Marc Szafraniec, Vasil Khalidov, Pierre Fernandez, Daniel HAZIZA, Francisco Massa, Alaaeldin El-Nouby, Mido Assran, Nicolas Ballas, Wojciech Galuba, Russell Howes, Po-Yao Huang, Shang-Wen Li, Ishan Misra, Michael Rabbat, Vasu Sharma, Gabriel Synnaeve, Hu Xu, Herve Jegou, Julien Mairal, Patrick Labatut, Armand Joulin, and Piotr Bojanowski. DINOv2: Learning robust visual features without supervision. *TMLR*, 2024. 1
- [30] Robin Rombach, Andreas Blattmann, Dominik Lorenz, Patrick Esser, and Björn Ommer. High-resolution image synthesis with latent diffusion models. In *Proceedings of the IEEE/CVF conference on computer vision and pattern recognition*, pages 10684–10695, 2022. 5

- [31] Olga Russakovsky, Jia Deng, Hao Su, Jonathan Krause, Sanjeev Satheesh, Sean Ma, Zhiheng Huang, Andrej Karpathy, Aditya Khosla, Michael Bernstein, Alexander C. Berg, and Li Fei-Fei. Imagenet large scale visual recognition challenge, 2015. 3
- [32] Tim Salimans and Jonathan Ho. Progressive distillation for fast sampling of diffusion models. *arXiv preprint arXiv:2202.00512*, 2022. 3
- [33] Tim Salimans, Ian Goodfellow, Wojciech Zaremba, Vicki Cheung, Alec Radford, and Xi Chen. Improved techniques for training gans. *Advances in neural information processing systems*, 29, 2016. 5
- [34] Florian Schroff, Dmitry Kalenichenko, and James Philbin. Facenet: A unified embedding for face recognition and clustering. In *2015 IEEE Conference on Computer Vision and Pattern Recognition (CVPR)*, page 815823. IEEE, 2015. 3
- [35] Rahul Shenoy, Zhihong Pan, Kaushik Balakrishnan, Qisen Cheng, Yongmoon Jeon, Heejune Yang, and Jaewon Kim. Gradient-free classifier guidance for diffusion model sampling. *arXiv preprint arXiv:2411.15393*, 2024. 3
- [36] Jiaming Song, Chenlin Meng, and Stefano Ermon. Denoising diffusion implicit models. In *International Conference on Learning Representations*, 2021. 2, 3
- [37] Jiaming Song, Qinsheng Zhang, Hongxu Yin, Morteza Mardani, Ming-Yu Liu, Jan Kautz, Yongxin Chen, and Arash Vahdat. Loss-guided diffusion models for plug-and-play controllable generation. In *International Conference on Machine Learning*, pages 32483–32498. PMLR, 2023. 3
- [38] Arash Vahdat, Karsten Kreis, and Jan Kautz. Score-based generative modeling in latent space, 2021. 3
- [39] Tianwei Yin, Michaël Gharbi, Taesung Park, Richard Zhang, Eli Shechtman, Fredo Durand, and William T Freeman. Improved distribution matching distillation for fast image synthesis. *arXiv preprint arXiv:2405.14867*, 2024. 3
- [40] Tianwei Yin, Michaël Gharbi, Richard Zhang, Eli Shechtman, Fredo Durand, William T Freeman, and Taesung Park. One-step diffusion with distribution matching distillation. In *Proceedings of the IEEE/CVF Conference on Computer Vision and Pattern Recognition*, pages 6613–6623, 2024. 3
- [41] Sihyun Yu, Sangkyung Kwak, Huiwon Jang, Jongheon Jeong, Jonathan Huang, Jinwoo Shin, and Saining Xie. Representation alignment for generation: Training diffusion transformers is easier than you think, 2024. 1, 2, 3, 5, 6, 7, 8
- [42] Min Zhao, Fan Bao, Chongxuan Li, and Jun Zhu. Egsde: Unpaired image-to-image translation via energy-guided stochastic differential equations. *Advances in Neural Information Processing Systems*, 35:3609–3623, 2022. 3
- [43] Mingyuan Zhou, Zhendong Wang, Huangjie Zheng, and Hai Huang. Long and short guidance in score identity distillation for one-step text-to-image generation. *arXiv preprint arXiv:2406.01561*, 2024. 3